ELSEVIER

Journal of Organometallic Chemistry 523 (1996) 153–165

Journal of Organometallic Chemistry

Counter anion effect on molecular structures of some iodobiruthenocenium and iodoferrocenylruthenocenium salts

Masanobu Watanabe *, Izumi Motoyama, Toshio Takayama

Department of Chemistry, Faculty of Engineering, Kanagawa University, Rokkakubashi, Yokohama 221, Japan

Received 10 January 1996; in revised form 17 April 1996

Abstract

Oxidations of biruthenocene (RcRc) and ferrocenylruthenocene (FcRc) with an equivalent amount of iodine or iodoruthenocenium $^+Y^-$ ($[RcHI]^+Y^-$), $Y = BF_4^-$ and PF_6^-) gave monocationic halometallocenium salts formulated as $[M^{II}Cp(C_5H_4C_5H_4)CpRu^{IV}I]^+Y^-$ ($M = Ru$, $Y = I_3$ **1**, BF_4 **2**; $M = Fe$, $Y = I_3$ **3**, BF_4 **4**, PF_6 **5**). The crystal structures of **1**, **3** and **4** were analyzed by single-crystal X-ray diffraction. The crystal of **1** is monoclinic, space group $P2_1/c$, $a = 10.737(3)$, $b = 23.957(3)$, $c = 9.936(3)$ Å, $\beta = 110.96(2)°$, $Z = 4$, final $R = 0.084$. The crystal of **3** is monoclinic, space group $P2_1/c$, $a = 10.575(3)$, $b = 23.811(6)$, $c = 9.902(4)$ Å, $\beta = 110.85(3)°$, $Z = 4$, final $R = 0.049$. The crystal of **4** is orthorhombic, space group $P2_12_12_1$, $a = 9.871(10)$, $b = 25.581(10)$, $c = 7.810(3)$ Å, $Z = 4$, final $R = 0.094$. The most interesting structural difference between the I_3^- (**1**, **3**) and other salts (**2**, **4**, **5**) is found in the direction of the Ru^{IV}–I bond with respect to the remaining half of the $M^{II}Cp(C_5H_4)$ ($M = Ru$, Fe) moiety. Because one end of the I_3^- anion sits above the C_5H_4 plane of the $M^{II}Cp(C_5H_4)$ moiety, the Ru^{IV}–I^- bond is fixed in the *trans* position to the $M^{II}Cp(C_5H_4)$ moiety, avoiding steric hindrance between them when the I_3^- salts (**1** and **3**) are crystallized. In the case of the BF_4^- and PF_6^- salts, the Ru^{IV}–I^- bond sits in the *cis* position to the $M^{II}Cp(C_5H_4)$ moiety, as shown in Scheme 1, and this conformation gives larger tilting angles between the two η^5-Cp and η^5-C_5H_4 on the Ru^{IV} side (e.g. tilting angles 42.40° and 39.21° for **2** and **4** respectively) than those of both I_3^- salts (31.08° for **1**, 32.73° for **3**) due to the van der Waals contact between I and the $C_5H_4C_5H_4$ plane. Such large conformational differences between the salts **1**, **3** and **2**, **4**, **5** were observed from the results of ^{13}C CP/MAS NMR and ^{57}Fe-Mössbauer spectroscopic studies; i.e. large temperature dependent ^{57}Fe-Mössbauer spectra were found for **4** and **5**, unlike the case of **3**, probably because of the delocalization of the higher positive $[IRu^{IV}Cp(C_5H_4)]^+$ charge to the $Fe^{II}Cp(C_5H_4)$ moiety for **4** and **5**.

Keywords: Ruthenium; Iron; Metallocenes

1. Introduction

Recently, the crystal structure of **2**, formulated as $[Ru^{II}Cp(C_5H_4C_5H_4)CpRu^{IV}I]^+BF_4^-$ has been determined by the present authors using X-ray analysis [1]. Two interesting structural features are found in the cation. One is the larger tilted structure of the η^5-Cp and η^5-C_5H_4 planes in the $[(C_5H_4)CpRu^{IV}I]^+$ moiety. The tilting angle between them is 42.40°, which is much larger than that of iodoruthenocenium $^+I_3^-$ ($[RcHI]^+I_3^-$) salt (32.2°) [2]. The other is the non-planarity of the $C_5H_4C_5H_4$ plane (the dihedral angle between the two C_5H_4 planes is 19.35°). As shown in Fig. 1, the Ru^{IV}–I bond is fixed in the *cis* position to the other half of the $Ru^{II}Cp(C_5H_4)$ moiety, thus these structural features may be caused by steric hindrance between the I and two C_1 atoms (the $I \cdots C(6)$ (3.188(8) Å) and

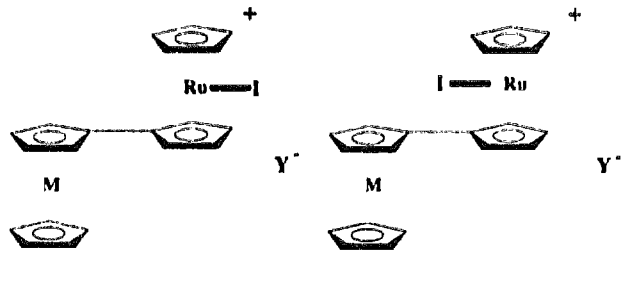

1; Ru Y; I_3
3; Fe Y; I_3

2; Ru Y; BF_4
4; Fe Y; BF_4
5; Fe Y; PF_6

Scheme 1.

* Corresponding author.

0022-328X/96/$15.00 © 1996 Elsevier Science S.A. All rights reserved
PII S0022-328X(96)06408-X

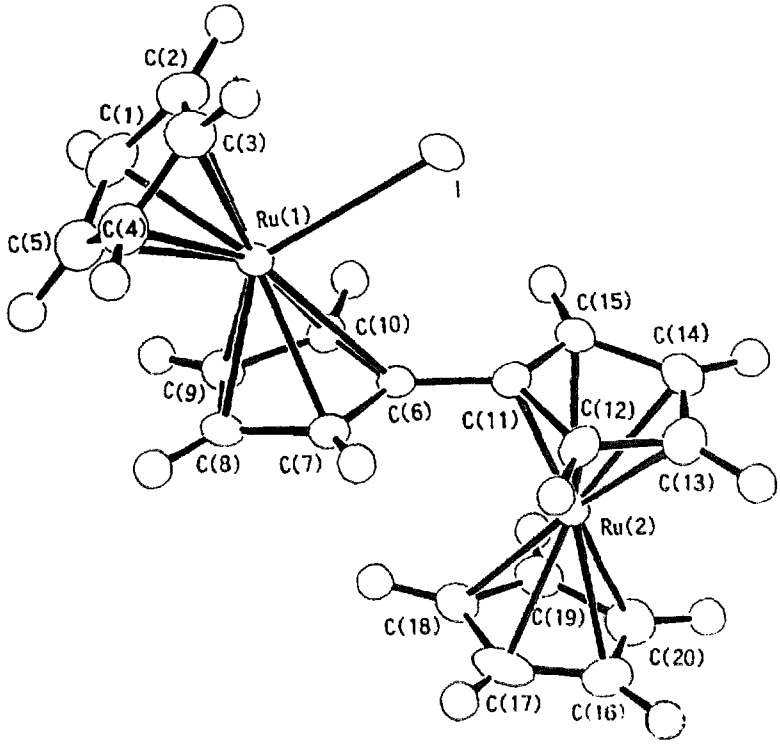

Fig. 1. ORTEP drawing of cation 2.

I···C(11) (3.253(9) Å) distances are much smaller than the sum of the van der Waals radii of C and I (3.85 Å)). To confirm this conclusion and widen our studies, the related salts **1** and **3**–**5** were prepared and their ^{13}C CP/MAS NMR and ^{57}Fe-Mössbauer spectroscopies carried out. The results of the measurements indicated the presence of structural differences between them; e.g. although **3** gives ferrocene-like ^{57}Fe-Mössbauer spectra at all the temperatures, **4** and **5** give temperature dependent ferrocene and ferrocenium-like spectra, suggesting some interaction between the $[IRu^{IV}Cp(C_5H_4)]^+$ and $Fe^{II}Cp(C_5H_4)$ moieties for the latter salts. Such counter anion effects were observed only in the solid state (the effect was found to be absent in solution, based on the results of ^1H NMR spectroscopy in CD_3COCD_3). It is therefore important to investigate the crystal structures of **1**, **3** and **4** in comparison with that of **2**. The aim of the present work is to discuss the different results of ^{57}Fe-Mössbauer and ^{13}C CP/MAS NMR studies from a structural point of view.

2. Experimental

2.1. Measurements

^{57}Fe-Mössbauer measurements were carried out using a $^{57}Co(Rh)$ source moving in constant acceleration mode. The isomer shift (IS) value was referred to metallic iron foil. The Mössbauer parameters were obtained by least-squares fitting to Lorentzian peaks. The experimental error of the IS and quadrupole splitting (QS) values was 0.02 mm s^{-1}. The ^{13}C CP/MAS NMR measurements were carried out by the method reported previously [3].

2.2. X-ray crystallography

Salts **1**, **3**, **4** and **5** were prepared by the method reported previously [4]. Crystals ($0.1 \times 0.1 \times 0.3$ mm^3) of **1**, ($0.1 \times 0.1 \times 0.3$ mm^3) of **3** and ($0.03 \times 0.2 \times 0.3$ mm^3) of **4** were selected. X-ray diffraction experiments were carried out on a Rigaku AFC-6A automated four-circle X-ray diffractometer with graphite monochromated Mo Kα radiation ($\lambda = 0.71073$ Å). The intensity data were collected at $25 \pm 1°$ using the ω–2θ scan mode with a scanning speed of 4° min^{-1}. The lattice parameters were determined by a least-squares calculation with 25 reflections. Crystal stability was checked by recording three standard reflections every 150 reflections, and no significant variations were observed. For **1**, 6847 reflections were collected in the range $4° \leq 2\theta \leq 55°$, 6483 were unique ($R_{int} = 0.054$), of which 2811 reflections with $I_{obs} > 2.5\sigma(I_{obs})$ were used for the structure determination. The scan width was $1.15 + 0.3 \tan \theta$. The refinement of 237 variable parameters converged to $R = \Sigma \| F_o | - | F_c \| / \Sigma | F_o | = 0.084$, $R_w = [\Sigma w(| F_o | - | F_c |)^2 / \Sigma w F_o^2)]^{1/2} = 0.105$, where $w = 4Lp^2F_o^2/[S^2(C + R^2B) + (pF_o^2)^2]$ (where S = scan rate, C = total integrated peak count, R = ratio of scan

Table 1
Crystal and intensity collection data for **1**, **3** and **4**

	1	**3**	**4**
Formula	$C_{20}H_{18}I_4Ru_2$	$C_{20}H_{18}FeI_4Ru$	$C_{20}H_{18}BF_4FeIRu$
Formula weight	968.12	922.90	628.99
Space group	$P2_1/c$	$P2_1/c$	$P2_12_12_1$
a (Å)	10.737(3)	10.575(3)	9.871(10)
b (Å)	23.957(3)	23.811(6)	25.581(10)
c (Å)	9.936(3)	9.902(4)	7.810(3)
β (°)	110.96(2)	110.85(3)	—
V (Å^3)	2386(1)	2329(1)	1972(2)
Z	4	4	4
D_x (g cm^{-3})	2.694	2.631	2.118
T (°C)	23	23	23
λ (Å)	0.71073	0.71073	0.71073
μ (cm^{-1})	64.45	65.76	31.06
No. of ref.	6483	5157	3287
No. of obs.	2811 ($I > 2.5\sigma(I)$)	2646 ($I > 2\sigma(I)$)	1272 ($I > 2.5\sigma(I)$)
R	0.084	0.049	0.094
R_w	0.105	0.046	0.102

time to background counting time, B = total background count, Lp = Lorentz-polarization factor and p = p-factor). The standard deviation s of an observation of unit weight was 2.53. For **3**, 5459 reflections were collected in the range $4° \leqq 2\theta \leqq 55°$, 5157 were unique ($R_{int} = 0.038$), of which 2646 reflections with $I_{obs} > 2\sigma(I_{obs})$ were used for the structure determination. The scan width was 1.15 + 0.3 tan θ. The refinement of 235 variable parameters converged to $R = 0.049$, $R_w = 0.046$, and $s = 1.93$. For **4**, 3287 reflections were collected in the range $4° \leqq 2\theta \leqq 60°$, of which 1272 reflections with $I_{obs} > 2.5\sigma(I_{obs})$ were used for the structure determination. The scan width was 0.84 + 0.3 tan θ. The refinement of 253 variable parameters converged to $R = 0.094$, $R_w = 0.102$ and $s = 2.37$.

The non-hydrogen atoms were refined anisotropically by full-matrix least-squares. For **1** and **4**, hydrogen atoms were fixed at the calculated positions, and for **3** the atoms were located from the difference of Fourier maps. Neutral atom scattering factors were taken from Cromer and Waber [5]; anomalous dispersion effects corrections were included in F_{calc} [6], the values for $\Delta f'$ and $\Delta f''$ were those of Creagh and McAuley [7]. All calculations were performed using the TEXSAN crystallographic software package [8]. Crystallographic data for **1**, **3** and **4** and some of the experimental conditions for the X-ray structure analysis are listed in Table 1.

3. Results and discussion

3.1. Salts 1 and 2

The results of single-crystal X-ray studies of **1** compared with studies of **2** are discussed first. The final atomic coordinates and equivalent isotropic temperature factors B_{eq} of non-hydrogen atoms, interatomic distances, and selected bond lengths and angles for **1** are shown in Tables 2, 3 and 4, and ORTEP drawings of the cation are shown in Fig. 2 with the atom numbering system. The cation of **1** is in *trans* conformation as with neutral RcRc and **2** [1], i.e. the two Ru atoms sit on opposite sides of the planar $C_5H_4C_5H_4$ ligand. The Ru(1) ··· Ru(2) distance (5.273(3) Å, which is ca. 0.2 Å smaller than the value for **2** (5.464(4) Å)) shows no interaction between them. The Ru(1)–I bond length is found to be 2.756(2) Å, which is 0.039 and 0.024 Å longer than the corresponding values for the cation **2** and $[RcHI]^+I_3^-$ respectively. The mean bond distances from Ru(1) to the ring carbon atoms (Ru(1)–C_{ring}) and to the cyclopentadienyl rings (Ru(1)–Cp) are 2.21(4) and 1.861(6) Å respectively, which are closer to those of the $[IRu^{IV}Cp(C_5H_4)]^+$ moiety of **2** (2.22(2) and 1.879(7) Å respectively). Similarly, mean Ru(2)–C_{ring} (2.11(1) Å) and Ru(2)–Cp (1.740(3) Å) bond distances are closer to the values of the Rc moiety of **2** (2.18(1) and 1.812(3) Å respectively). Thus, the cation can be formulated as $[Ru^{II}Cp(C_5H_4C_5H_4)CpRu^{IV}I]^+$.

The most essential difference between **1** and **2** is found in the direction of the Ru^{IV}–I^- bond to the other half of the Rc moiety. As shown in Fig. 2, I sits in *trans* position to the Rc moiety. Therefore, a much larger distance Ru(2)–I (7.697(3) Å) and angle I(1)Ru(1)Ru(2) (145.2°) were found compared with the values for cation **2** (5.398(5) Å and 105.8° respectively). Moreover, η^5-C_5H_4 (C(6–10) plane) shows good planarity (the deviations of all C atoms from the least-squares plane are within the range 0.0012–0.0038 Å), owing to the absence of steric hindrance between I(1) and C(6), unlike the case of **2**, where the η^5-C_5H_4 ring is non-planar

Table 2
Atomic coordinates and isotropic temperature factors for 1

Atom	x	y	z	B_{eq} [a] (Å^2)
I(1)	−0.5783(2)	−0.28454(7)	−0.3418(2)	5.0
I(2)	−0.4999(2)	−0.05585(8)	0.1896(2)	5.7
I(3)	−0.2545(2)	−0.11069(7)	0.1996(2)	4.7
I(4)	−0.0114(2)	−0.16995(6)	0.2082(2)	6.3
Ru(1)	−0.4793(2)	−0.17808(7)	−0.3365(2)	2.5
Ru(2)	−0.0485(2)	−0.05814(9)	−0.2648(2)	3.8
C(1)	−0.560(4)	−0.094(1)	−0.368(6)	7.0
C(2)	−0.651(4)	−0.128(2)	−0.472(4)	7.3
C(3)	−0.696(3)	−0.164(1)	−0.398(5)	6.2
C(4)	−0.642(5)	−0.159(2)	−0.261(6)	9.4
C(5)	−0.549(4)	−0.110(2)	−0.234(4)	8.6
C(6)	−0.281(2)	−0.136(1)	−0.308(2)	2.6
C(7)	−0.335(2)	−0.164(1)	−0.446(3)	3.5
C(8)	−0.344(2)	−0.222(1)	−0.420(3)	3.5
C(9)	−0.297(2)	−0.228(1)	−0.271(3)	3.5
C(10)	−0.260(2)	−0.177(1)	−0.205(2)	3.3
C(11)	−0.247(2)	−0.077(1)	−0.287(2)	2.7
C(12)	−0.245(2)	−0.037(1)	−0.392(2)	3.5
C(13)	−0.180(2)	0.011(1)	−0.325(3)	3.4
C(14)	−0.138(2)	0.004(1)	−0.173(2)	3.1
C(15)	−0.177(2)	−0.051(1)	−0.147(2)	2.9
C(16)	0.051(3)	−0.131(1)	−0.288(4)	5.8
C(17)	0.055(3)	−0.093(1)	−0.391(3)	5.0
C(18)	0.120(2)	−0.046(1)	−0.324(3)	4.3
C(19)	0.162(2)	−0.053(1)	−0.180(3)	4.3
C(20)	0.123(2)	−0.105(1)	−0.146(3)	4.9

[a] $B_{eq} = 4/3(B_{11}a^2 + B_{22}b^2 + B_{33}c^2 + B_{13}ac\cos\beta)$. B_{ij}s are defined by $\exp[-(h^2B_{11} + k^2B_{22} + l^2B_{33} + 2klB_{23} + 2hlB_{13} + 2hkB_{12})]$.

(the dihedral angle between the plane C(6)–C(7)–C(10) and C(7–10) being 11.60°).

The interplane C(1) ··· C(6), C(2) ··· C(7), C(3) ··· C(8), C(4) ··· C(9) and C(5) ··· C(10) distances are found to be 3.00(4), 3.40(5), 4.10(4), 4.10(6) and 3.40(5) Å respectively. The largest distance (4.10 Å) is closer to the value for $[RcHI]^+ I_3^-$ (4.11(3) Å) [2], thus a similar tilting angle between the η^5-Cp and

Table 3
Selected interatomic distances for 1

Atom 1	Atom 2	Distance (Å)	Atom 1	Atom 2	Distance (Å)
Ru(1)	I(1)	2.756(2)	Ru(1)	Ru(2)	5.273(3)
I(2)	I(3)	2.914(3)	I(3)	I(4)	2.944(3)
Ru(1)	C(1)	2.17(3)	Ru(1)	C(2)	2.21(3)
Ru(1)	C(3)	2.21(3)	Ru(1)	C(4)	2.19(3)
Ru(1)	C(5)	2.18(3)	Ru(1)	C(6)	2.28(2)
Ru(1)	C(7)	2.21(2)	Ru(1)	C(8)	2.18(2)
Ru(1)	C(9)	2.18(3)	Ru(1)	C(10)	2.25(2)
Ru(2)	C(11)	2.11(2)	Ru(2)	C(12)	2.09(2)
Ru(2)	C(13)	2.11(2)	Ru(2)	C(14)	2.14(2)
Ru(2)	C(15)	2.12(2)	Ru(2)	C(16)	2.10(2)
Ru(2)	C(17)	2.13(2)	Ru(2)	C(18)	2.11(2)
Ru(2)	C(19)	2.11(2)	Ru(2)	C(20)	2.11(2)
C(1)	C(2)	1.40(5)	C(1)	C(5)	1.35(5)
C(2)	C(3)	1.35(5)	C(3)	C(4)	1.28(5)
C(4)	C(5)	1.50(5)	C(6)	C(7)	1.45(3)
C(6)	C(10)	1.39(3)	C(7)	C(8)	1.44(3)
C(8)	C(9)	1.38(3)	C(9)	C(10)	1.36(3)
C(6)	C(11)	1.45(3)	C(11)	C(12)	1.42(3)
C(11)	C(15)	1.46(3)	C(12)	C(13)	1.38(3)
C(13)	C(14)	1.42(3)	C(14)	C(15)	1.43(3)
C(16)	C(17)	1.37(4)	C(16)	C(20)	1.49(4)
C(17)	C(18)	1.38(4)	C(18)	C(19)	1.35(3)
C(19)	C(20)	1.39(4)			

Table 4
Selected bond lengths (Å) and angles (deg) for 1–4

	1	2	3	4
M^{II} [a] ··· Ru^{IV}	5.273(3)	5.464(4)	5.219(2)	5.324(6)
M^{II}–Cp [b]	1.740(3)	1.812(3)	1.649(9)	1.649(19)
Ru^{IV}–Cp [c]	1.861(6)	1.879(7)	1.864(9)	1.840(28)
M^{II}–C_{ring} (av)	2.11(1)	2.18(1)	2.03(6)	2.03(6)
Ru^{IV}–C_{ring} (av)	2.21(4)	2.22(2)	2.21(9)	2.21(9)
Ru^{IV}–I	2.756(2)	2.717(2)	2.731(2)	2.746(1)
C_{ring}–C_{ring} (Fe)	1.41(3)	1.40(6)	1.41(4)	1.42(1)
C_{ring}–C_{ring} (Ru)	1.39(3)	1.37(9)	1.42(5)	1.42(3)
Dihedral angle				
Cp–Ru^{IV}–C_5H_4	31.08	42.40	32.73	39.21

[a] M = Ru for 1, 2 and Fe for 3, 4.
[b] Fe–Cp; the distance between the Fe and η^5-Cp and η^5-C_5H_4 rings.
[c] Ru–Cp; the distance between the Ru and η^5-Cp and η^5-C_5H_4 rings.

η^5-C_5H_4 planes of the Ru^{IV} side will be expected; actually the value is found to be 31.08° (32.2° for the $[RcHI]^+$ cation). Therefore, the larger tilting angle between the rings (42.4°) found in cation **2** is verified by the steric hindrance between the I and two C_1 atoms (C(6) and C(11)), and as a result the non-planarity of the $C_5H_4C_5H_4$ plane is observed in cation **2**.

The structure of the Rc moiety of **1** is similar to that of **2**; i.e. the η^5-Cp and η^5-C_5H_4 rings are nearly parallel (tilting angle 1.44°) and the mean interplane C_{ring} ··· C_{ring} distance of the Rc moiety is 3.41(9) Å. As shown in Fig. 2 (upper part), the η^5-Cp and η^5-C_5H_4 rings of the Rc moiety are essentially eclipsed, as in the case of RcH and the $[RcHI]^+$ cation (rotation angle 1.2(9)°), while the two tilting rings on the Ru^{IV} side are in a nearly intermediate eclipsed and staggered state (rotation angle ca. 20(2)°), as with **2**.

A stereo view of the packing down the *c* axis of **1** is shown in Fig. 3. The unit has an asymmetric I_3^- anion (I(2)–I(3)–I(4); distances I(2)–I(3) and I(3)–I(4) 2.914(3) and 2.944(3) Å respectively; I(2)–I(3)–I(4) angle 178.0(1)° i.e. the anion is I_2–I^- in character). The shortest intermolecular I(1) ··· I(2) and I(1) ··· I(3) distances are 3.904(3) and 4.188(2) Å respectively; these values are less than the value (4.30 Å) of the van der Waals radii of two I atoms [9]; i.e. I(1) is in contact with I_3^-. However, an absence of contact between I_3^- anions is found (the shortest intermolecular I_3^-–I_3^- distance (4.622(4) Å) is much longer than the sum of the van der Waals radii of two I atoms [9]).

The characteristic feature of the packing is found in the position of the I_3^-; i.e. the I_3^- sits perpendicularly above the C_5H_4 plane (C(11–15)) of the Rc moiety. Fig. 4 gives a space filling plot, showing the contact between the I_3^- and cation **1**. Although the I(2)* ··· C(13)* (4.26(2)), I(2)* ··· C(14)* (4.03(2)) and I(2)* ··· C(15)* (4.21(2) Å) distances are longer than the sum of the van der Waals radii of I and C atoms (3.85 Å) [9], this packing decides the structure of the cation **1**; i.e. avoiding steric hindrance between I(1) and the bulky I_3^-, the direction of the Ru^{IV}–I^- bond is fixed as the *trans* position to the Rc moiety when the salt **1** is crystallized. The absence of BF_4^- on the Ru^{II} side of the C_5H_4 plane and a demand for close packing between

Table 5
Dihedral angles between planes (deg)

Plane	C(6)–C(10)	C(11)–C(15)	C(16)–C(20)
Compound 1			
C(1–5)	31.08	17.02	15.75
C(6–10)	—	14.06	15.36
C(11–15)	—	—	1.44
Compound 3			
C(1)–C(5)	32.73	18.48	16.93
C(6)–C(10)	—	14.25	15.87
C(11)–C(15)	—	—	2.01
Compound 4			
C(1)–C(5)	39.21	46.08	42.03
C(6)–C(10)	—	21.32	17.81
C(11)–C(15)	—	—	4.52

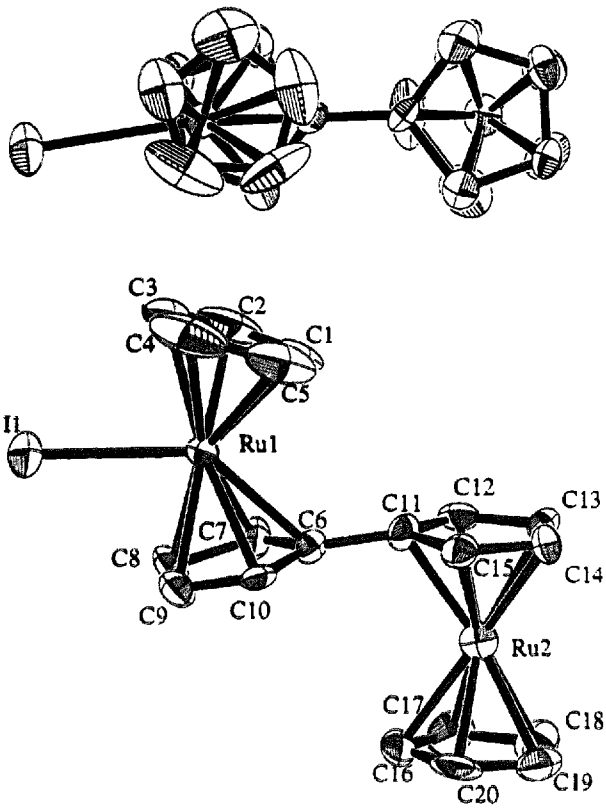

Fig. 2. ORTEP drawing of cation **1** with thermal ellipsoids at the 40% probability level: perspective view with atomic numbering scheme (bottom), projection of a whole molecule onto the Cp plane (top).

the cation and anion, means that the direction of the Ru^{IV}–I^- bond is fixed as the *cis* position to the Re moiety for **2**, as shown in Fig. 1. These structural

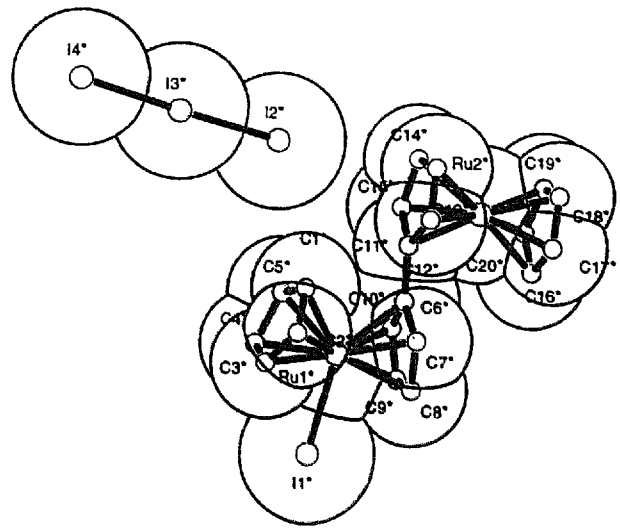

Fig. 4. Space filling plot showing the contact between I_3^- and the cation **1**.

differences, caused by the counter ions, are also reflected in the results of solid state NMR.

Fig. 5 shows ^{13}C CP/MAS NMR spectra of (a) **1** and (b) **2**. Two sharp signals are observed for both the salts. For **1**, the lower field ^{13}C signal at δ 93.5 is ascribed to the Cp- and C_5H_4-ring ($C_{2,5}$ positions) of the Ru^{IV} side, and at δ 78.0 to those of the Ru^{II} side. The reason for the smaller peak intensity of the Ru^{IV} side compared with that of the Ru^{II} side is explained by the overlapping of the other C_5H_4-ring signal ($C_{3,4}$ positions) of the Ru^{IV} side to the Ru^{II} signal on the basis of ^{13}C NMR spectroscopy in solution [4]. All attempts to find the C_1 signals of the Ru^{II} and Ru^{IV}

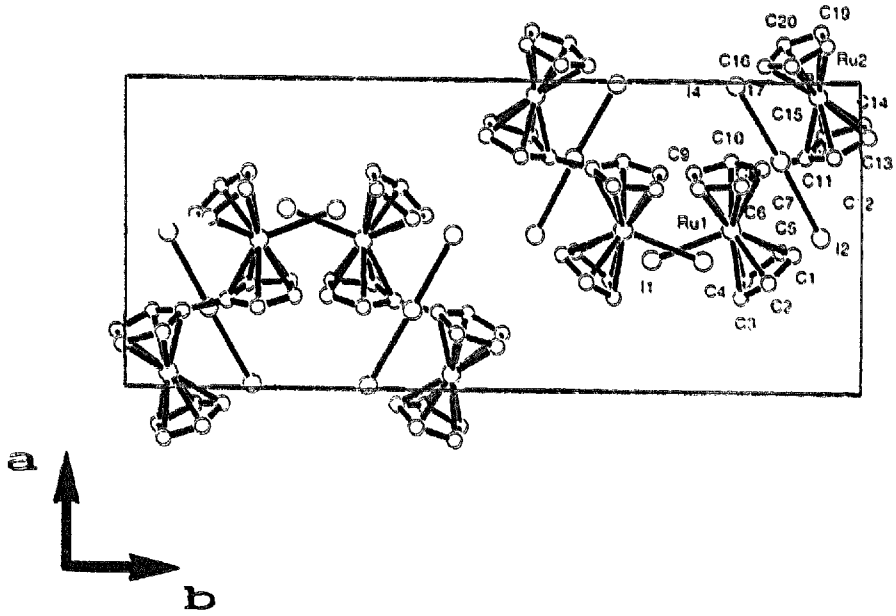

Fig. 3. Projection of the unit cell of **1** along the *c* axis.

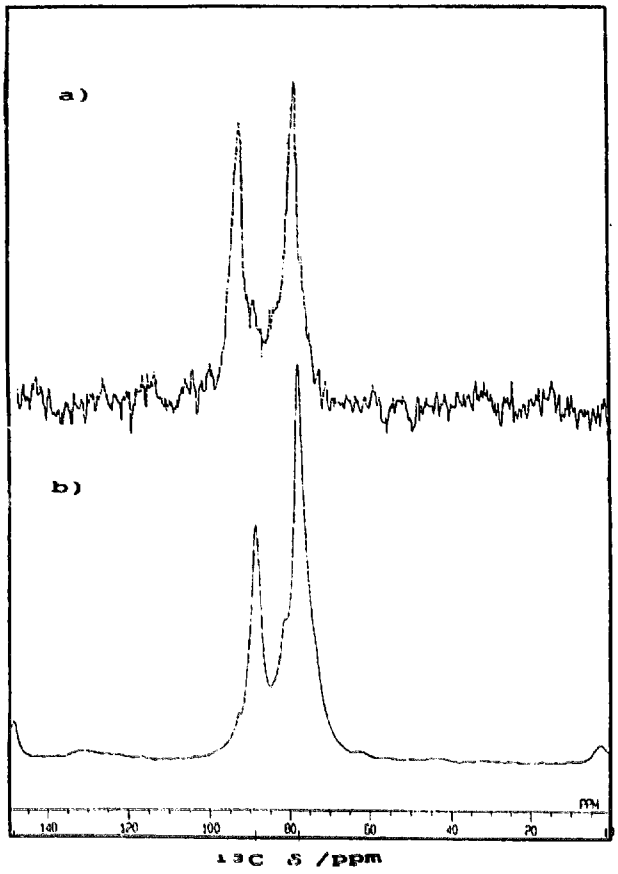

Fig. 5. ^{13}C CP/MAS NMR spectra of (a) **1** and (b) **2**.

sides have been unsuccessful because of their poor intensities. For **2**, ring carbon signals of the Ru^{II} side are observed at δ 77.7, those of the Ru^{IV} side at δ 88.7, which is a higher field shift (ca. $\Delta\delta = 4.8$) compared with the value of **1** because of the structure difference between them. I is in van der Waals contact with the C_5H_4-ring of the Ru^{II} side for **2**, thus the higher positive charge of Ru^{IV} may be delocalized over Ru^{IV}–$I\cdots C_5H_4CpRu^{II}$, resulting in the higher field shift observed in the $[IRu^{IV}Cp(C_5H_4)]^+$ moiety. In contrast, the absence of such contact in **1** gives no higher field shift of the Ru^{IV} side.

As described in the Introduction, these counter anion effects are observed only in the solid state. From results of ^1H NMR spectroscopy of **1** in CD_3COCD_3, the absence of the counter anion effect was observed [10]; i.e. **1** gives six sharp signals in CD_3COCD_3 at 183 K; δ 6.41 (2H), 6.05 (5H), 5.76 (2H), 5.33 (2H), 5.19 (2H) and 4.61 (5H). The former three signals are assigned as ring protons of the $[IRu^{IV}Cp(C_5H_4)]^+$ moiety, and the latter three signals as the $Ru^{II}Cp(C_5H_4)$ moiety. The same δ values are observed for the analogous BF_4^- **2** and PF_6^- salts, implying no interaction between the anion and the cation in solution. Avoiding steric hindrance between the I and two C_1 atoms in the $C_5H_4C_5H_4$ ligand in solution, the direction of the Ru^{IV}–I bond may be fixed as the *trans* position to the Rc moiety in acetone, as for **1** in solid. In order to estimate the central metal positive charge, ^{57}Fe-

Table 6
Atomic coordinates and isotropic temperature factors for **3**

Atom	x	y	z	B_{eq} [a] (Å^2)
I(1)	0.0858(1)	−0.21513(5)	−0.1572(1)	5.1
I(2)	−0.0073(1)	0.05501(5)	0.1875(1)	5.5
I(3)	0.2397(1)	0.10960(4)	0.1952(1)	4.0
I(4)	0.4862(1)	0.16975(6)	0.2046(1)	6.1
Ru	−0.0155(1)	−0.32093(4)	−0.1617(1)	2.3
Fe	−0.4471(2)	−0.44110(7)	−0.2325(2)	2.1
C(1)	0.061(2)	−0.4049(7)	−0.131(3)	5.4
C(2)	0.058(2)	−0.3906(9)	−0.264(2)	6.6
C(3)	0.146(2)	−0.3426(9)	−0.095(3)	5.8
C(5)	0.152(2)	−0.3734(9)	−0.025(2)	5.6
C(6)	−0.217(1)	−0.3642(5)	−0.186(1)	2.1
C(7)	−0.237(1)	−0.3226(6)	−0.296(1)	2.9
C(8)	−0.202(1)	−0.2698(5)	−0.227(2)	3.3
C(9)	−0.154(1)	−0.2785(5)	−0.078(1)	2.6
C(10)	−0.162(1)	−0.3352(6)	−0.051(1)	3.0
C(11)	−0.257(1)	−0.4220(5)	−0.210(1)	2.3
C(12)	−0.321(1)	−0.4483(5)	−0.345(1)	2.6
C(13)	−0.363(1)	−0.5023(5)	−0.320(2)	3.0
C(14)	−0.322(1)	−0.5092(6)	−0.170(1)	3.0
C(15)	−0.256(1)	−0.4601(5)	−0.098(1)	2.3
C(16)	−0.542(1)	−0.3685(6)	−0.218(2)	4.2
C(17)	−0.610(1)	−0.3934(8)	−0.349(2)	4.7
C(18)	−0.654(1)	−0.4460(7)	−0.325(1)	3.3
C(19)	−0.611(1)	−0.4537(6)	−0.176(2)	3.7
C(20)	−0.544(1)	−0.4050(7)	−0.108(2)	3.9

[a] $B_{eq} = 4/3(B_{11}a^2 + B_{22}b^2 + B_{33}c^2 + B_{13}ac\cos\beta)$. B_{ij}s are defined by $\exp[-(h^2B_{11} + k^2B_{22} + l^2B_{33} + 2klB_{23} + 2hlB_{13} + 2hkB_{12})]$.

Mössbauer spectroscopy and X-ray diffraction studies were carried out using salts **3–5**.

3.2. Salts 3–5

The results of X-ray studies of **3** are discussed first. Tables 6 and 7 show the final atomic coordinates and equivalent isotropic temperature factors B_{eq} of non-hydrogen atoms and selected bond lengths for **3** respectively. Fig. 6 is a ORTEP drawing of the cation **3**. The structure of the cation is similar to that of **1**; i.e. the direction of the Ru–I bond is *trans* to the Fe moiety. The Ru–I, Fe · · · Ru and Fe · · · I distances are found to be 2.731(2), 5.219(2) and 7.492(2) Å respectively. These values correspond well with the values for **1** (2.756(2), 5.273(3) and 7.697(3) Å respectively). The I–Ru · · · Fe angle (138.7°) is 6.5° smaller than that for **1**.

The mean Ru–Cp and Ru–C_{ring}, Fe–Cp and Fe–C_{ring} distances are 1.864(9) and 2.21(9), 1.649(9) and 2.03(6) Å respectively. The former two values are closer to the values for the $[IRu^{IV}Cp(C_5H_4)]^+$ moiety of **1**, and the latter two values to those for ferrocene (1.65 and 2.045 Å) [11]. Thus the oxidation states of Ru and Fe are assigned formally as Ru^{IV} and Fe^{II}; i.e. the formula of the cation is given as $[Fe^{II}Cp(C_5H_4C_5H_4)CpRu^{IV}I]^+$, as already verified using ^{57}Fe-Mössbauer spectroscopy [12]. The tilting angle between the Cp and C_5H_4 planes on the Re moiety is 32.73° (2.01° for the Fe moiety), this is slightly larger than the value for **1**. As in the case of **1**, the Cp and C_5H_4 planes of the Fe moiety are eclipsed (the rotation angle between them is ca. 1(1)°).

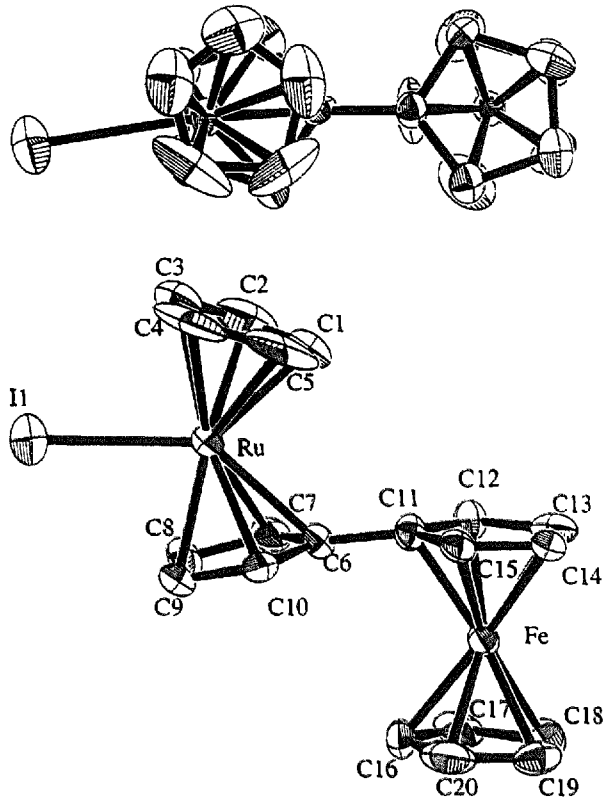

Fig. 6. ORTEP drawing of cation **3** with thermal ellipsoids at the 40% probability level: perspective view with atomic numbering scheme (bottom), projection of a whole molecule onto the Cp plane (top).

These two planes of the Re moiety are in an intermediate eclipsed and staggered state (the rotation angle between them is ca. 19(2)°). The packing of the cation

Table 7
Selected interatomic distances for **3**

Atom 1	Atom 2	Distance (Å)	Atom 1	Atom 2	Distance (Å)
Ru	I(1)	2.731(2)	Ru	Fe	5.219(2)
I(2)	I(3)	2.894(2)	I(3)	I(4)	2.946(2)
Ru	C(1)	2.14(2)	Ru	C(2)	2.21(2)
Ru	C(3)	2.18(1)	Ru	C(4)	2.21(2)
Ru	C(5)	2.19(1)	Ru	C(6)	2.30(1)
Ru	C(7)	2.24(1)	Ru	C(8)	2.21(1)
Ru	C(9)	2.17(1)	Ru	C(10)	2.22(1)
Fe	C(11)	2.00(1)	Fe	C(12)	2.03(1)
Fe	C(13)	2.05(1)	Fe	C(14)	2.04(1)
Fe	C(15)	2.04(1)	Fe	C(16)	2.03(1)
Fe	C(17)	2.04(1)	Fe	C(18)	2.05(1)
Fe	C(19)	2.03(1)	Fe	C(20)	2.05(1)
C(1)	C(2)	1.35(3)	C(1)	C(5)	1.37(2)
C(2)	C(3)	1.32(3)	C(3)	C(4)	1.37(3)
C(4)	C(5)	1.33(2)	C(6)	C(7)	1.43(2)
C(6)	C(10)	1.43(2)	C(7)	C(8)	1.41(2)
C(8)	C(9)	1.40(2)	C(9)	C(10)	1.38(2)
C(6)	C(11)	1.43(2)	C(11)	C(12)	1.42(2)
C(11)	C(15)	1.43(2)	C(12)	C(13)	1.41(2)
C(13)	C(14)	1.41(2)	C(14)	C(15)	1.42(2)
C(16)	C(17)	1.38(2)	C(16)	C(20)	1.40(2)
C(17)	C(18)	1.38(2)	C(18)	C(19)	1.39(2)
C(19)	C(20)	1.40(2)			

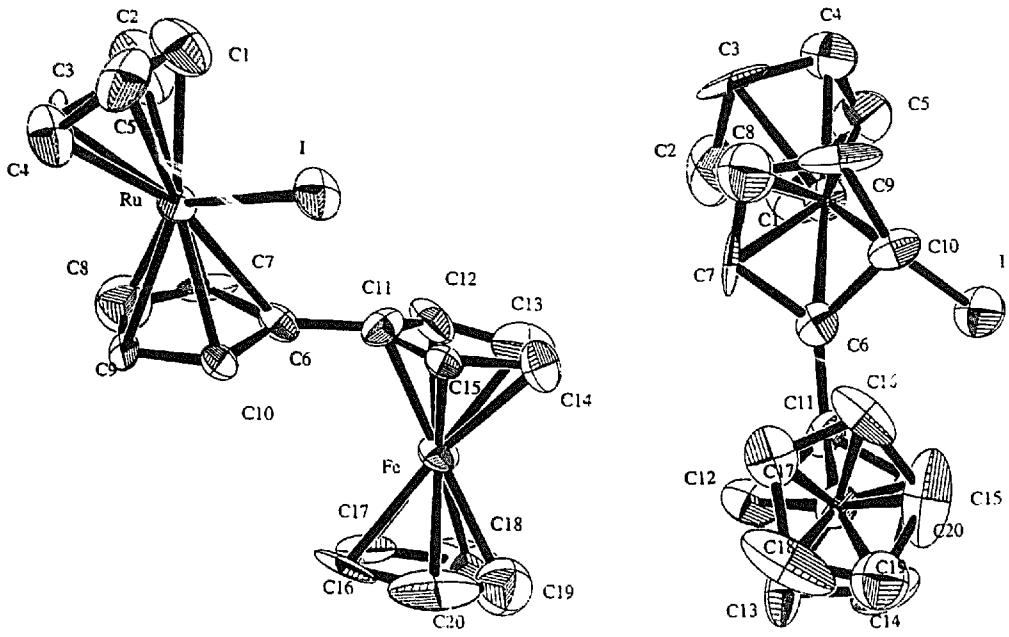

Fig. 7. ORTEP drawing of cation 4 with thermal ellipsoids at the 40% probability level: perspective view with atomic numbering scheme (bottom), projection of a whole molecule onto the Cp plane (top).

and I_3^- is the same as with **1**; i.e. the I_3^- sits on the C_5H_4 plane (C(11–15)) of the Fc moiety (the shortest I(2) to C atoms distance is 3.94(1) Å (I(2)* $\cdots$ C(13)*)). All the crystal data of **3** indicate that its crystal structure is homologous to that of **1**.

In contrast, the crystal data of **4** is different from that of **2**; e.g. the space groups of **2** and **4** are $P2_1/n$ and $P2_12_12_1$ respectively and the cell parameters of **2** (a = 25.078(12), b = 10.599(12), c = 7.652(8) Å, β = 95.17(8)°) are different from those of **4** (a = 9.871(10),

Table 8
Atomic coordinates and isotropic temperature factors for **4**

Atom	x	y	z	B_{eq} [a] (Å^2)
I	0.0839(4)	0.1433(1)	0.1722(3)	4.5
Ru	0.2074(4)	0.1821(1)	−0.1157(4)	2.9
Fe	−0.0049(6)	0.0010(2)	−0.3166(7)	2.8
F(1)	0.504(5)	0.183(3)	0.472(6)	14.7
F(2)	0.676(5)	0.151(1)	0.359(4)	11.2
F(3)	0.613(4)	0.135(1)	0.630(4)	10.3
F(4)	0.692(6)	0.210(1)	0.556(5)	11.2
C(1)	0.376(6)	0.202(2)	0.067(6)	6.2
C(2)	0.278(8)	0.242(1)	0.072(6)	7.4
C(3)	0.255(7)	0.263(2)	−0.080(6)	6.6
C(4)	0.373(5)	0.235(3)	−0.166(8)	11.6
C(5)	0.415(5)	0.192(2)	−0.093(7)	13.5
C(6)	0.118(4)	0.104(1)	−0.243(4)	2.3
C(7)	0.224(4)	0.128(2)	−0.333(5)	4.7
C(8)	0.185(5)	0.178(2)	−0.388(4)	12.7
C(9)	0.048(6)	0.188(2)	−0.309(6)	5.8
C(10)	0.006(5)	0.146(2)	−0.220(5)	5.4
C(11)	0.111(4)	0.052(2)	−0.187(4)	4.7
C(12)	0.005(4)	0.031(2)	−0.078(4)	2.8
C(13)	0.025(6)	−0.025(2)	−0.069(5)	5.6
C(14)	0.141(4)	−0.037(2)	−0.183(5)	4.2
C(15)	0.188(4)	0.010(2)	−0.239(5)	3.3
C(16)	−0.125(5)	0.038(2)	−0.497(6)	5.2
C(17)	−0.182(6)	0.011(3)	−0.390(7)	8.2
C(18)	−0.196(7)	−0.023(4)	−0.398(5)	12.3
C(19)	−0.094(9)	−0.053(3)	−0.498(9)	20.3
C(20)	−0.027(4)	−0.001(4)	−0.568(7)	11.3
B	0.621(5)	0.171(2)	0.514(5)	3.4

[a] $B_{eq} = 4/3(B_{11}a^2 + B_{22}b^2 + B_{33}c^2 + B_{13}ac\cos\beta)$. B_{ij}s are defined by $\exp[-(h^2B_{11} + k^2B_{22} + l^2B_{33} + 2klB_{23} + 2hlB_{13} + 2hkB_{12})]$.

$b = 25.581(10)$, $c = 7.810(3)$ Å). Fig. 7 shows an ORTEP drawing of the cation of **4** formulated as $[Fe^{II}Cp(C_5H_4C_5H_4)CpRu^{IV}I]^+$. The distance between Fe^{II} and Ru^{IV} is 5.324(6) Å, which is ca. 0.14 Å smaller than the value for **2**, as shown in Table 9. The mean $Fe-C_{ring}$ (1.649(19)), Fe–Cp (2.03(6)), $Ru-C_{ring}$ (1.840(28)) and Ru–Cp (2.21(9) Å) distances agree with the corresponding values for **3**. The most interesting structural feature of the cation is the direction of the Ru–I bond to the C_5H_4 plane of the Fc moiety; I is coordinated to Ru from the oblique side of the Fc moiety. The torsion angle I–Ru–C(6)–C(11) is 43.0(1)°, while the angle for **3** is small (9(1)°; the same value is found for **1**). The $I \cdots C(6)$ distance (3.386(1) Å) is longer than the value for **2** (3.188(8) Å), suggesting less steric hindrance between I and C(6). The smaller tilting angle (39.21°) between the Cp and C_5H_4 rings of the Ru^{IV} side, and the lesser non-planarity of the C_5H_4 plane of the Ru^{IV} side compared with those of **2**, are explained by the same reason.

Fig. 8 shows ^{13}C CP/MAS NMR spectra of (a) **3** and (b) **4**. For **3**, two broad main ^{13}C peaks ($\delta = 93.1$ and 75.8) are observed. On the basis of previous studies, the signal at lower field is ascribed to the Cp and $C_{2,5}$ of the $[Cp(C_5H_4)Ru^{IV}I]^+$ moiety, and the signal at higher field to the $Cp(C_5H_4)Fe^{II}$ moiety. The much larger peak intensity of the latter is explained by the same reason described for **1** and **2**. For **4**, three broad main signals ($\delta = 89.4$, 75.9 and 73.1) are observed; the lower field signal ($\delta = 89.4$) is ascribed to the Cp and $C_{2,5}$ of the $[IRu^{IV}Cp(C_5H_4)]^+$ moiety, the higher signal

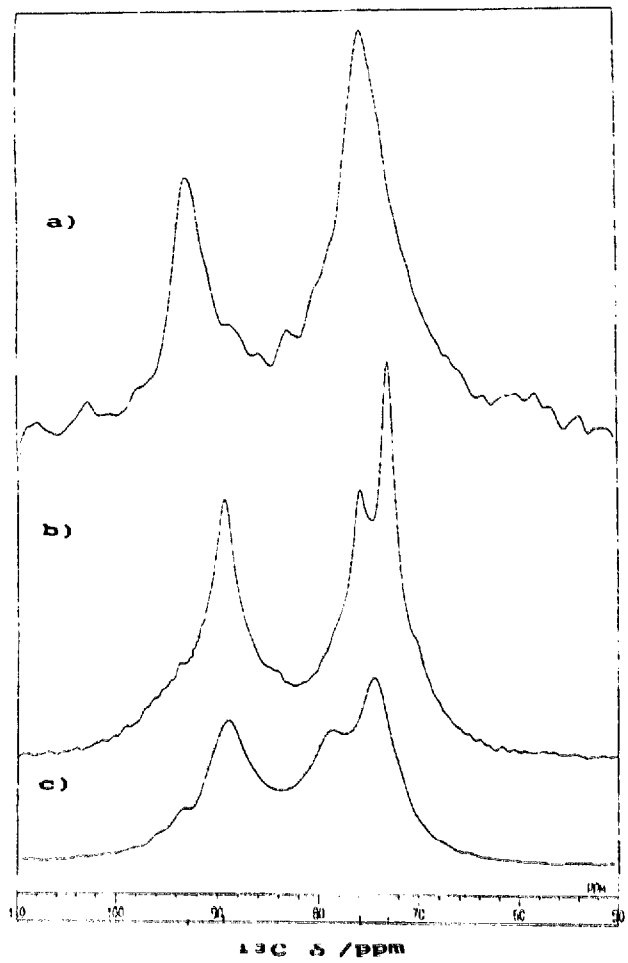

Fig. 8. ^{13}C CP/MAS NMR spectra of (a) **3**, (b) **4** and (c) **5**.

Table 9
Selected interatomic distances for **4**

Atom 1	Atom 2	Distance (Å)	Atom 1	Atom 2	Distance (Å)
Ru	I(1)	2.745(4)	Ru	Fe	5.324(6)
B	F(1)	1.24(6)	B	F(2)	1.40(5)
B	F(3)	1.29(5)	B	F(4)	1.26(6)
Ru	C(1)	2.24(5)	Ru	C(2)	2.22(4)
Ru	C(3)	2.13(5)	Ru	C(4)	2.15(5)
Ru	C(5)	2.09(5)	Ru	C(6)	2.41(3)
Ru	C(7)	2.23(4)	Ru	C(8)	2.14(2)
Ru	C(9)	2.23(5)	Ru	C(10)	2.36(4)
Fe	C(11)	2.00(4)	Fe	C(12)	2.03(3)
Fe	C(13)	2.07(4)	Fe	C(14)	2.03(4)
Fe	C(15)	2.00(4)	Fe	C(16)	2.08(4)
Fe	C(17)	1.96(8)	Fe	C(18)	2.04(5)
Fe	C(19)	2.12(6)	Fe	C(20)	1.98(5)
C(1)	C(2)	1.42(8)	C(1)	C(5)	1.38(3)
C(2)	C(3)	1.32(5)	C(3)	C(4)	1.45(9)
C(4)	C(5)	1.35(8)	C(6)	C(7)	1.42(5)
C(6)	C(10)	1.44(9)	C(7)	C(8)	1.44(7)
C(8)	C(9)	1.49(8)	C(9)	C(10)	1.38(7)
C(6)	C(11)	1.37(5)	C(11)	C(12)	1.49(5)
C(11)	C(15)	1.37(5)	C(12)	C(13)	1.46(6)
C(13)	C(14)	1.48(6)	C(14)	C(15)	1.35(6)
C(16)	C(17)	1.36(7)	C(16)	C(20)	1.43(8)
C(17)	C(18)	1.34(7)	C(18)	C(19)	1.39(7)
C(19)	C(20)	1.40(5)			

($\delta = 73.1$) to the Cp and $C_{3,4}$ of the Fc moiety, and the signal ($\delta = 75.9$) to the $C_{3,4}$ (Ru side) and $C_{2,5}$ (Fe side). The higher field shift ($\Delta\delta$ ca. 4 ppm) is also observed for the $[IRu^{IV}Cp(C_5H_4)]^+$ moiety in **4** owing to the same reason described previously for **2** compared with **1**.

Fig. 9 shows ^{57}Fe-Mössbauer spectra of (a) **4** and (b) the related PF_6 salt **5** at the indicated temperatures. Although no temperature dependence was observed for **3** (IS 0.52, QS 2.16 mm s^{-1} at 78 K; IS 0.43, QS 2.16 mm s^{-1} at 300 K), significant temperature dependence is observed for **4**; i.e. the two types of Fe atom are observed at 300 K. One is a large portion of a ferrocene-like component (IS 0.43, QS 2.05) and the other is a small portion of a ferrocenium-like one (IS 0.43). At decreasing temperatures, the intensity of the Fe^{III} component decreases and only the Fe^{II} component (IS 0.51, QS 2.20 mm s^{-1}) remains at 78 K. Such temperature dependence of the ^{57}Fe-Mössbauer spectra is observed remarkably for **5**, with the ^{57}Fe-Mössbauer spectrum at 78 K showing a ferrocene-like doublet (QS 2.13, IS 0.50 mm s^{-1}) accompanied by a broad singlet of ferrocenium character (IS 0.45 mm s^{-1}). The areal intensity ratio (Fe(III)/(Fe(II) + Fe(III)) κ is ca. 0.14. With increasing temperature, a decreasing ferrocene-like line (QS 1.97, IS 0.44 mm s^{-1}) and increasing ferrocenium-like line (QS 0.37, IS 0.42 mm s^{-1}) are observed, the κ value is found to be ca. 0.46 (for **4** the κ value is ca. 0.20 at 300 K); i.e. the oxidation state of the Fe atom in **5** is closer to that of ferrocenium compared with the case of **3** (Fe^{II}) and **4**. This result corresponds well with that of the ^{13}C CP/MAS NMR spectra. Because of the paramagnetic ferrocenium species, three broader ^{13}C CP/MAS NMR signals (δ = 88.8, 74.4 and 78.6) were found for **5**, as shown in Fig. 8(c). The lower field signal ($\delta = 88.8$) is ascribed to the Cp and $C_{2,5}$ ring carbons of the $[IRu^{IV}Cp(C_5H_4)]^+$ moiety and the other two signals to the Rc and $C_{3,4}$ ring carbons of the $[IRu^{IV}Cp(C_5H_4)]^+$ moiety.

Although X-ray diffraction studies of **5** have been carried out, the final R (0.12) and standard deviation values are too large to describe because of a lack of success in preparing single crystals of suitable size and the larger thermal motion of PF_6^-. However, it is still useful to discuss the structure of **5** in comparison with that of **4**. The crystal form of **5** is $P4_1$, $a = 10.72(1)$, $c = 18.60(2)$ Å, $V = 2137$ Å^3 and $Z = 4$. The conformation of the cation is quite similar to that of **2**; the Ru–I bond (2.741(6) Å) sits just above the C_5H_4 plane of the Fc moiety, unlike the case of **4**. The torsion angle I–Ru–C(6)–C(11) is negligible. The I · · · C(6) distance (3.286(6) Å) is much smaller (ca. 0.3 Å) than the value

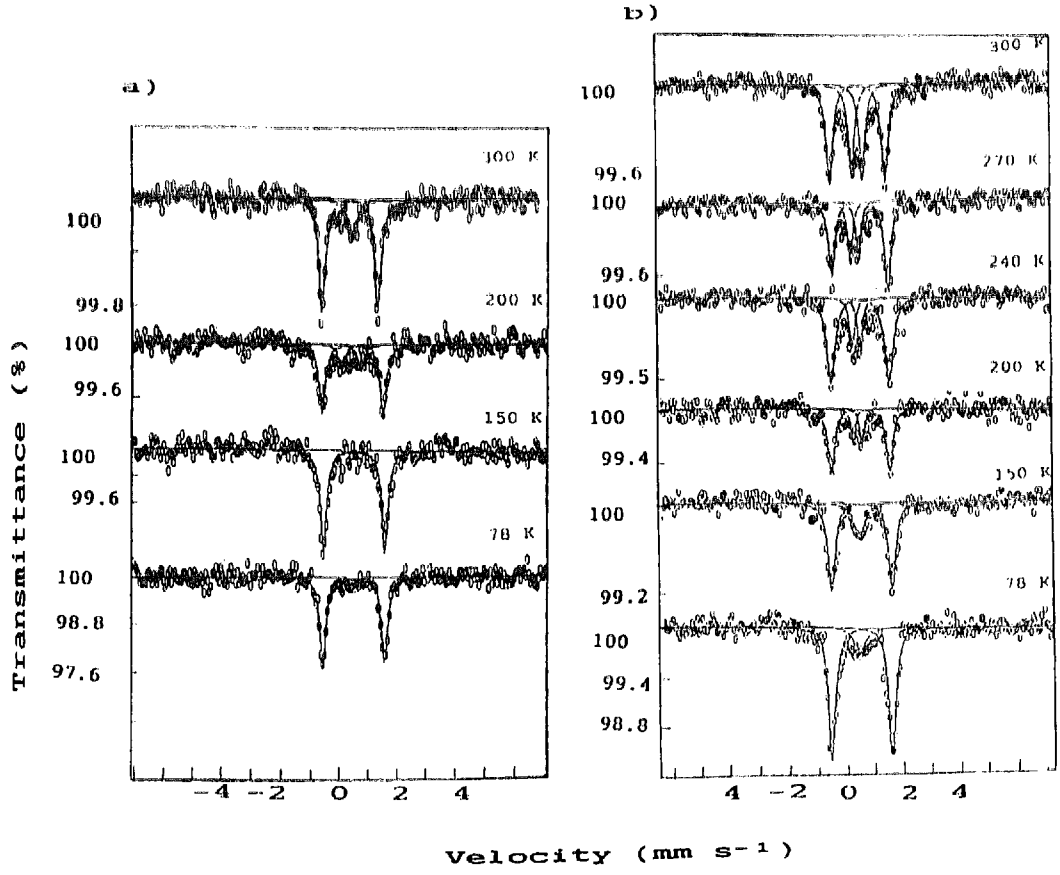

Fig. 9. ^{57}Fe-Mössbauer spectra of (a) **4** and (b) **5** at the indicated temperatures.

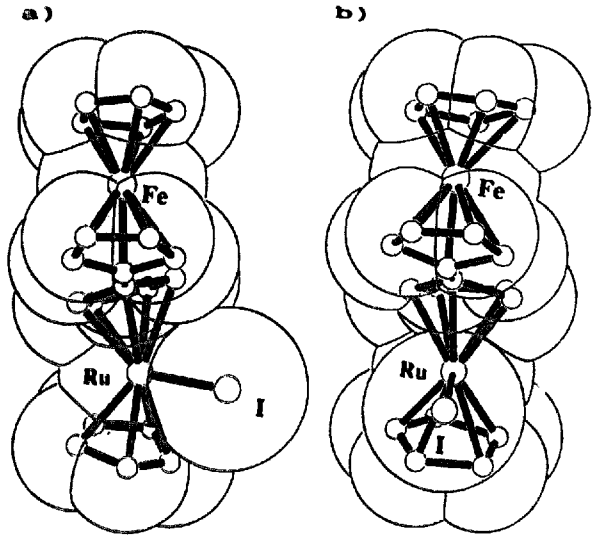

Fig. 10. Space filling plot showing the difference in structure of cations **4** (a) and **5** (b).

for **4**; i.e. the coordinated I atom sits closer to the C_5H_4 plane of the Fe moiety (van der Waals contact), as shown in Fig. 10(b), unlike the case of **3** and **4**. That conformational change may be deeply concerned with the results of ^{57}Fe-Mössbauer spectra for **3–5**.

For the last two decays, ^{57}Fe-Mössbauer spectroscopic and X-ray studies have been reported on the mixed-valence 1',1'''-dialkylbiferrocenium and 1',1'''-dihalobiferrocenium salts [13–17]. Results of the ^{57}Fe-Mössbauer spectroscopy of 1',1'''-diethylbiferrocenium$^+I_3^-$ and biferrocenium$^+I_3^-$ indicate the presence of significant interaction between the Cp or C_5H_4 planes and I_3^- (van der Waals contact between the Cp-ring and I atom), which is the driving force for the temperature dependence of the Mössbauer spectra. Moreover, Konno et al. [15] concluded that the van der Waals contact between the halogen atoms (X = I, Br) and the other C_5H_4 plane of the fulvalene moiety is the driving force for the averaged valence state of the mixed-valence 1',1'''-diiodo- and 1',1'''-dibromobiferrocenium salts, even at low temperature (4.2 K) [15]. Considering these reported facts and the results of the present studies, it seems reasonable to conclude that the positive charge of Ru^{IV} is delocalized over $C_5H_4Ru^{IV}$–$I^- \cdots C_5H_4Fe^{II}$ through the overlap between I^- and the C_5H_4 plane, giving a larger portion of ferrocenium-like species for **5** at 300 K compared with **4**. With the absence of such an interaction, **3** gives ferrocene-like ^{57}Fe-Mössbauer spectra at all temperatures.

Like the case of **1** and **2**, the absence of a counter anion effect is observed in acetone with ^{1}H NMR spectroscopy; i.e. six sharp signals (δ 6.58 (2H), 5.97 (2H), 6.10 (5H), 5.05 (2H), 5.13 (2H) and 4.29 (5H)) are observed at 183 K for **3**. The former three signals are assigned as ring protons of $[IRu^{IV}Cp(C_5H_4)]^+$ and the latter three signals as the $Fe^{II}Cp(C_5H_4)$ moiety. Six quite similar signals were observed for **4** and **5** under the same conditions [18], implying that the direction of the Ru^{IV}–I bond is fixed as the *trans* position to the Fc moiety in solution.

From the results of the present study, it can be found that the structure of the cations **1–5** formulated as $[M^{II}Cp(C_5H_4C_5H_4)CpRu^{IV}I]^+$ is dependent on the counter anion effect (I_3^-, BF_4^- and PF_6^-). The direction of the Ru^{IV}–I bond is fixed as the *trans* position to the $M^{II}Cp(C_5H_4)$ moiety for I_3^- salt (**1**, **3**) avoiding steric hindrance between the bulky I_3^- and the Ru^{IV}–I bond. In the case of BF_4^- (**2**, **4**) and PF_6^- (**5**) salts, the Ru^{IV}–I bond is fixed as the *cis* position to the $M^{II}Cp(C_5H_4)$ moiety, which gives the large tilted structure found in the $[Cp(C_5H_4)Ru^{IV}I]^+$ moiety and the non-planarity of the $C_5H_4C_5H_4$ plane caused by the van der Waals contact between I and the C_5H_4-ring of the $M^{II}CpC_5H_4$ moiety. This contact gives the delocalization of the higher positive $[IRu^{IV}CpC_5H_4]^+$ charge to the $M^{II}CpC_5H_4$ moiety based on the results of ^{13}C CP/MAS and ^{57}Fe-Mössbauer spectroscopic studies.

References

[1] M. Watanabe, I. Motoyama, M. Shimoi and T. Iwamoto, *Inorg. Chem.*, *33* (1994) 2518.
[2] Y.S. Sohn, A.W. Schlüter, D.N. Hendrickson and H.B. Gray, *Inorg. Chem.*, *13* (1974) 301.
[3] M. Watanabe, I. Motoyama, T. Takayama, M. Shimoi and H. Sano, *J. Organomet. Chem.*, *496* (1995) 87.
[4] M. Watanabe, T. Iwamoto, A. Kubo, S. Kawata, H. Sano and I. Motoyama, *Inorg. Chem.*, *31* (1992) 177.
[5] D.T. Cromer and J.T. Waber, *International Table for X-ray Crystallography*, Vol. IV, Kynoch Press, Birmingham, UK, 1974, Table 2.2 A.
[6] J.A. Ibers and W.C. Hamilton, *Acta Crystallogr.*, *17* (1964) 781.
[7] D.C. Creagh and W.J. McAuley, *International Table for X-ray Crystallography*, Vol. C, Kluwer Academic, Boston, 1992, Table 4.2.6.8, pp. 219–222.
[8] *TEXSAN: Crystal Structure Analysis Package*, Molecular Structure Corp. 1985.
[9] L. Pauling, *The Nature of the Chemical Bond*, Cornell University Press, 3rd edn., 1960.
[10] M. Watanabe, T. Iwamoto and H. Sano, *J. Organomet. Chem.*, *446* (1993) 177.
[11] P. Seiler and J.D. Dunitz, *Acta Crystallogr.*, *B35* (1979) 1068.
[12] M. Watanabe, Y. Masude, I. Motoyama and H. Sano, *Bull. Chem. Soc. Jpn.*, *61* (1988) 827.
[13] T.-Y. Dong, D.N. Hendrickson, K. Iwai, M.J. Cohn, S.J. Geib, A.L. Rheingold, H. Sano, I. Motoyama and S. Nakashima, *J. Am. Chem. Soc.*, *107* (1985) 7996.
[14] T.-Y. Dong, D.N. Hendrickson, C.G. Pierpont and M.F. Moore, *J. Am. Chem. Soc.*, *108* (1986) 963.

[15] M. Konno, S. Hyodo and S. Iijima, *Bull. Chem. Soc. Jpn.*, *55* (1982) 2327; M. Konno and H. Sano, *Bull. Chem. Soc. Jpn.*, *61* (1988) 1455.
[16] M.J. Cohn, T.-Y. Dong, D.N. Hendrickson, S.J. Geob and A.L. Rheingold, *J. Chem. Soc., Chem. Comman.*, (1985) 1095.
[17] M.H. Morrison, Jr. and D.N. Hendrickson, *Inorg. Chem.*, *14* (1975) 2331.
[18] M. Watanabe, T. Iwamoto, H. Sano and I. Motoyama, *J. Organomet. Chem.*, *455* (1993) 197.